The Electrochemical Society
Advancing solid state & electrochemical science & technology

A Magnetite Composite of Molecularly Imprinted Polymer and Reduced Graphene Oxide for Sensitive and Selective Electrochemical Detection of Catechol in Water and Milk Samples: An Artificial Neural Network (ANN) Application

To cite this article: Hicham Meskher *et al* 2023 *J. Electrochem. Soc.* **170** 047502

View the article online for updates and enhancements.

You may also like

A Magnetite Composite of Molecularly Imprinted Polymer and Reduced Graphene Oxide for Sensitive and Selective Electrochemical Detection of Catechol in Water and Milk Samples: An Artificial Neural Network (ANN) Application

Hicham Meskher,[1,z] Samir Brahim Belhaouari,[2,z] Kalim Deshmukh,[3] Chaudhery Mustansar Hussain,[4] and Fariborz Sharifianjazi[5]

[1]*Division of Process Engineering, College of Applied Science, Kasdi-Merbah University, Ouargla, 30000, Algeria*
[2]*Division of Information and Computing Technology, College of Science and Engineering, Hamad Bin Khalifa University, Education City, Qatar Foundation, PO Box 34110, Doha, Qatar*
[3]*New Technologies - Research Center, University of West Bohemia, Plzeň 30100, Czech Republic*
[4]*Department of Chemistry and Environmental Science, New Jersey Institute of Technology, Newark, New Jersey 07102, United States of America*
[5]*School of Science and Technology, University of Georgia, Tbilisi, Georgia*

In the present study, a stable and more selective electrochemical sensor for catechol (CC) detection at magnetic molecularly imprinted polymer modified with green reduced graphene oxide modified glassy carbon electrode (MIP/rGO@Fe$_3$O$_4$/GCE). Two steps have been applied to achieve the imprinting process: (1) adsorption of CC on the surface of the polypyrrole (Ppyr) during the polymerization of pyrrole and (2) the green extraction of the template (CC) from the mass produced. Hence, the present paper doesn't present the first use of MIP technology for CC identification but, it presents a new extraction process. The MIP/rGO@Fe3O4/GCE was characterized by voltammetry techniques and exhibited a wide linear range from1 50 μM of CC while the detection limits were estimated to be around 4.18 nM CC and limit of quantification in the range of 12.69 nM CC. Furthermore, the prepared MIP-based sensor provided outstanding electroanalytical performances including high selectivity, stability, repeatability, and reproducibility. For the accurate estimation of CC concentrations, an artificial neural network (ANN) was developed based on the findings of the study. The MIP/rGO@Fe3O4/GCE exhibits excellent stability with a very important selectivity and sensitivity. The analytical testing of the modified electrode has been analyzed in water and commercial milk samples and provided adequate recoveries.

Recently, several chemical industries such as pharmaceuticals, pesticides, and cosmetics have been widely used catechol (CC) which is an isomer of dihydroxybenzene.[1,2] The US Environmental Protection Agency has listed CC as toxic compounds due to their effect on the environment and its resources, and the human health.[3–6] So, it is highly recommended to develop novel and accurate analytical tools to detect such toxic compounds.

So far, huge number of physicochemical analytical tools such as gas chromatography (GC) and liquid chromatography (LC) have been used to investigate CC.[7–12] These techniques are considered sensitive and accurate analytical tools however; they suffer from several drawbacks since they are time-consuming, complicated to operate, expensive, and need sample pretreatment. On the other hand, electrochemical techniques may overcome these challenges because they offer highly sensitive, simple, and more selective detection of CC and they don't require sample pretreatment. For this purpose, researchers and academics have used several nanomaterials to modify electrodes to improve their sensitivity to prepare electrochemical sensors.[13–15] Molecularly imprinted polymers (MIPs), as outstanding nanocomposites offer several advantages such as high selectivity, resistance toward high levels of pressure, temperature, and physicochemical changes.[16–19] MIPs are described as biomimetic molecules that can bind particularly to the analytes they are intended to detect. In the presence of the target molecule (template), MIPs are prepared through several techniques.[20] The binding sites preserve the specific characteristics of the studied molecule once it is removed from the synthesized MIP. The target analyte is recognized by the cavities created in the synthesized polymer.[21,22] MIP-based electrochemical sensors offer more selective determination of various analytes, including small molecules such as metals,[17,23]

acids,[24] waste water[25] as well as biological samples[26,27] even SARS-Cov-2 (COVID-19) detection.[28] Furthermore, machine learning offers several numerical simulations such as an artificial neural network that has been applied (ANN) to quantitatively anticipate and simulate sensor performance, in this regard, such models offer a great prediction of the undetected low concentrations. As result, ANN approaches have attracted the attention of researchers and academics to be used in different fields including healthcare,[29,30] water analysis,[31] environmental monitoring,[32] and lithium-ion battery state of charge assessment.[33] However, no scientific papers applied ANN to predict CC sensor low concentrations have been published so far. As a result, in the present study, the developed ANN has been used to predict low concentrations of CC. The predictions of the model under dynamical variables are provided and investigated.

Herein, we don't report only the first MIP-based sensor for an accurate and more selective identification of CC, but we report the first template extraction from the MIP through a green extraction process using citric acid extracted from a local fresh lemon. Meanwhile, to the best knowledge of the authors, this is the first study that reports a green reduction of graphene oxide using *Polygonum cognatum* extract. Furthermore, an accurate ANN has developed to predict CC concentrations provided by the developed sensor.

Materials and Methods

Reagents and instruments.—Catechol, graphite powder, dopamine (DA), hydroquinone (HQ), glucose (Gl), citric acid (CA) and cafeic acid (CAc), iron chloride (FeCl$_3$), Pyrrole (Pyr), sodium hydroxide (NaOH), monosodium and disodium phosphate, were obtained from Sigma-Aldrich. All chemicals were analytical grade and used in experiments without further purification.

At room temperature, the electrochemical measures have been carried out using a three-electrode system where was a saturated

[z]E-mail: hicham.meskher@g.enp.edu.dz; sbelhaouari@hbku.edu.qa
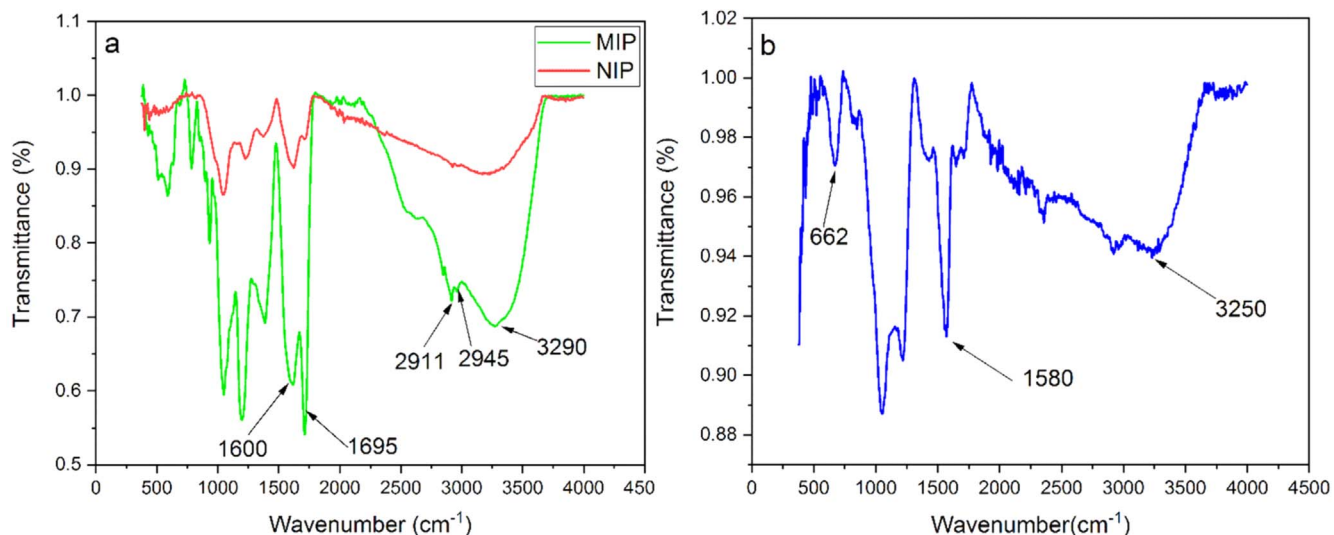
Figure 1. FTIR spectra of (a) magnetite MIP, NIP and, (b) rGO@Fe3O4 nanocomposites.
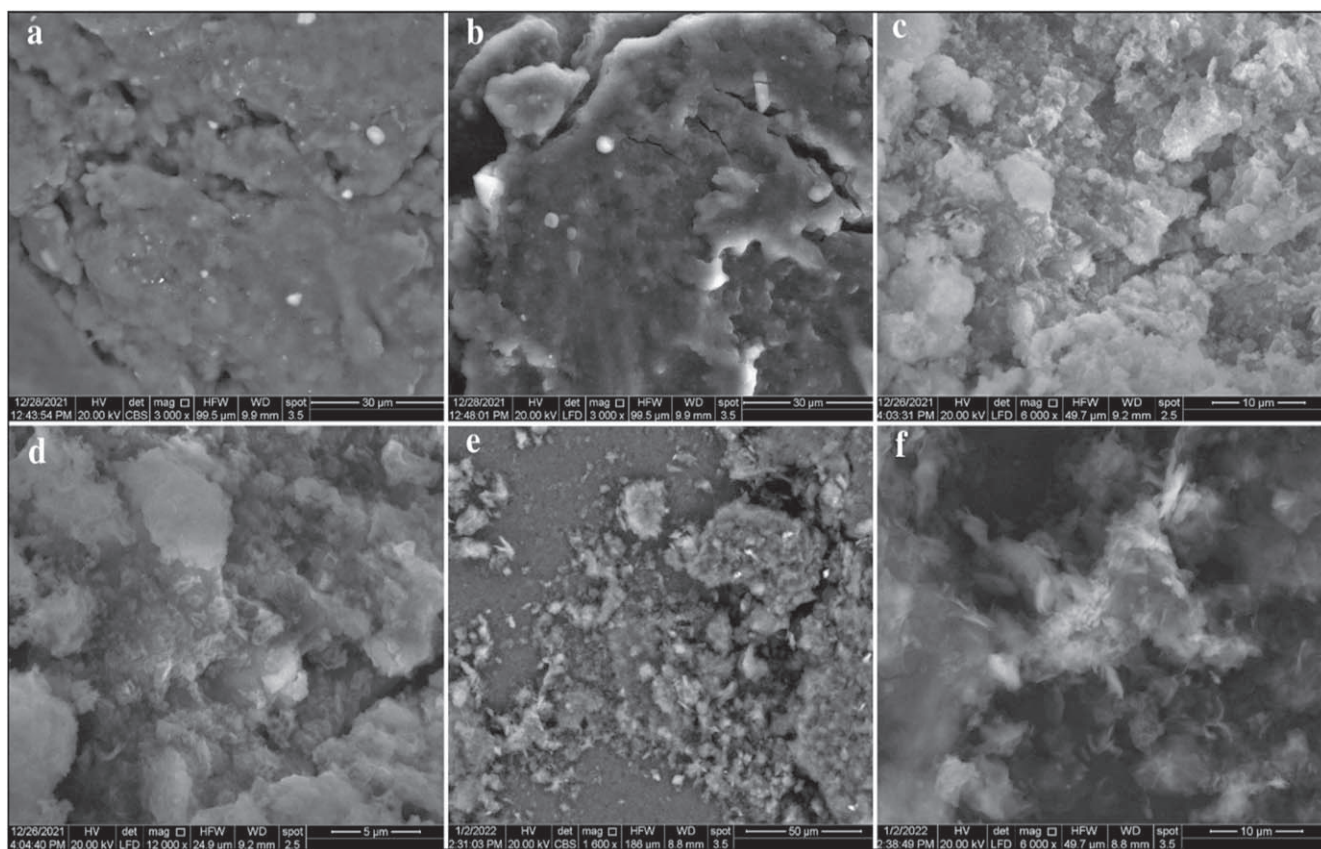
Figure 2. SEM analysis of (a), (b) magnetite NIP, (c), (d) magnetite MIP and, (e), (f) rGO@Fe_3O_4 nanocomposites.

calomel electrode (SCE) was used as a reference while a platinum wire a glassy carbon electrode (GCE) electrode used as counter and working electrode, respectively.

Electrochemical sensor preparation.— *Preparation of the modified electrodes.*—Before each operation, to clean and avoid creating grooves on its surface, the GCE electrode is polished using alumina slurry and then washed with deionized water (DW). For comparison with the bare GCE, 3 μl of the colloidal solution of the synthesized materials was drop-casted on the GCE to prepare four electrodes

namely rGO@Fe_3O_4/GCE, MIP/GCE, MIP/rGO@Fe_3O_4/GCE, and NIP/GCE.

Synthesis of green magnetic MIP.—Chemical polymerization of pyrrole with iron chloride ($FeCl_3 \cdot 6H_2O$) as the oxidant with presence of CC as molecule template, the MIP was synthesized. 1 g of ($FeCl_3 \cdot 6H_2O$) were dissolved in 200 ml of DW with presence of CC (30 mg). Then, 1 ml of Ppyr was added dropwise and the solution was stirred for 8 h at room temperature until a black color appears indicating the successful formation of polypyrrole (PPy). The mass
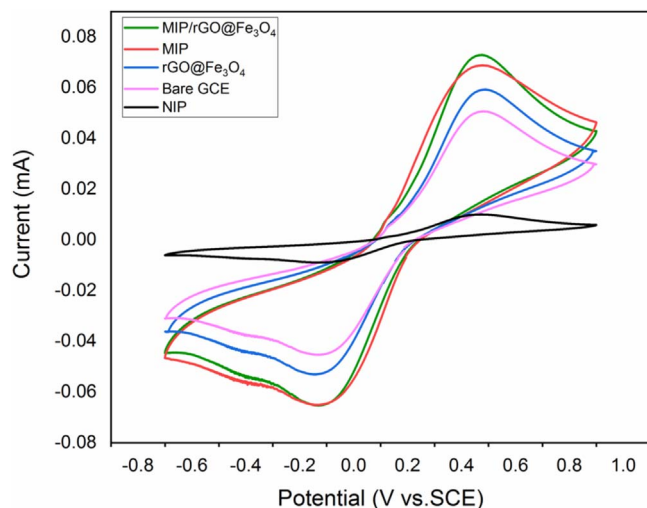
Figure 3. CVs of 5 mM ferri-ferrocyanide at the modified GCEs in 0.1 M PBS (pH 7) at scan rate of 0.1 V s^{-1}.

precipitated was collected and washed with a mixture of ethanol/citric acid (lemon) (1:2, v/v) to remove the template (CC) from the mass-produced and again with ethanol/water (1:1, v/v). Following the same steps, without using the template (CC), the non-imprinted polymer (NIP) was prepared. All collected masses have been dried for 12 h at 80 °C.

Preparation of magnetite reduced graphene oxide (rGO@Fe₃O₄).—As reducing and stabilizing agent, the aqueous extract of *Polygonum cognatum* has been used to prepare rGO@Fe$_3$O$_4$ the nanocomposite. Following identification, fresh *Polygonum cognatum* leaves were cleaned using DW to eliminate any undesired particles. After drying, the plant leaves were crushed into a fine powder. Leaf extract was made by combining 30 g of fine plant powder with 100 ml of purified water and heating it at 80 °C for around 35 min. After that, it was left at room temperature for 72 h. The leaf extract was filtered and kept at 4 °C for further use. For the synthesis of rGO@Fe$_3$O$_4$, 50 mg of GO was added to 50 ml of FeCl$_3$ (10 mM). The orange solution obtained was merged in 10 ml of *Polygonum cognatum* extract. After 15 min of magnetic stirring, the color of the mixture turned dark brownish indicating the successful formation reduction of GO. The acquired quantity was washed three times with distilled water to eliminate contaminants until the pH value reached 7, and the finished product was dried at a temperature of 25 °C for 72 h.

Electrochemical studies.—In this section, cyclic voltammetry (CV) to characterize the nanomaterials synthesized while differential pulse voltammetry (DPV) and amperometry (Amp) were carried out to study the electroanalytical performance and the selectivity of the fabricated sensor toward CC, respectively.

The development of the artificial neural network (ANN).—To predict CC concentrations, an artificial neural network (ANN) model was built. The model and program were built using the MATLAB R2017a Neural Network Toolbox (Mathworks, Natick, MA). Section 3 presents a detailed implementation of the concept.

Results and Discussion

Characterization of the prepared materials.—As shown in Fig. 1a, FTIR spectroscopy has been investigated characterize magnetic MIP and NIP. To confirm the presence of Ppyr, the sample was characterized by FTIR, the bands obtained are in good agreement with those reported in the literature for Ppyr.[34–36] Sharp vibrations around 2911 and 2962 cm^{-1} are –CH$_3$ or–CH$_2$ while the asymmetrical ester's vibrations appeared at 1165 and 1160 cm^{-1} and stretching vibrations of –OH appeared at 3285 and 3290 cm^{-1}. In addition, C=C stretching appeared at 1600 and 1695 cm^{-1} indicating the successful synthesis of MIP and NIP.[37] On the other hand, the stretching vibrations of O–H and C=C (Fig. 1b) appeared at 3250 and 1580 cm^{-1},[38,39] respectively and the band at 662 cm^{-1} represents the vibration of Fe–O.[40]

To evaluate the surface morphology of the synthesized nanomaterials, SEM analysis has been examined and the results obtained are presented in Fig. 2. Compared to MIP, Figs. 2a, 2b show that NIP has a smoother surface. However, the MIP has a rough and more porous surface with more cavities Figs. 2c, 2d, and thus, magnetite MIP has more affinity towards CC molecule compared to the NIP. As a result, the produced MIP promises good results regarding the selective determination of CC. SEM was used to describe the surface morphologies of rGO@Fe3O4 (Figs. 2e, 2f). Aside from the wrinkled layers, Figs. 2e, 2f show the dispersion of the iron oxide NPs and rGO surface. In the inset, Fig. 3 depicts the magnetic characteristics of rGO@Fe3O4, as well as the dispersion and agglomeration processes of rGO.
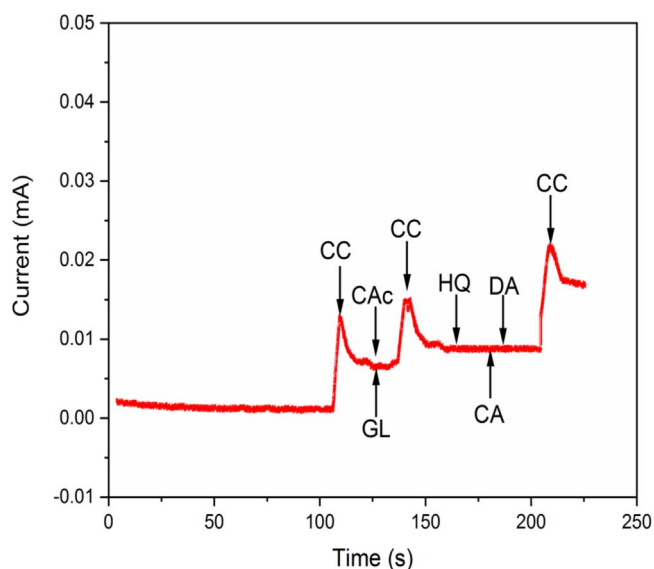
Electrochemical characterization of the synthesized nanomaterials.—The electrodes were characterized using CV in 5 mM of
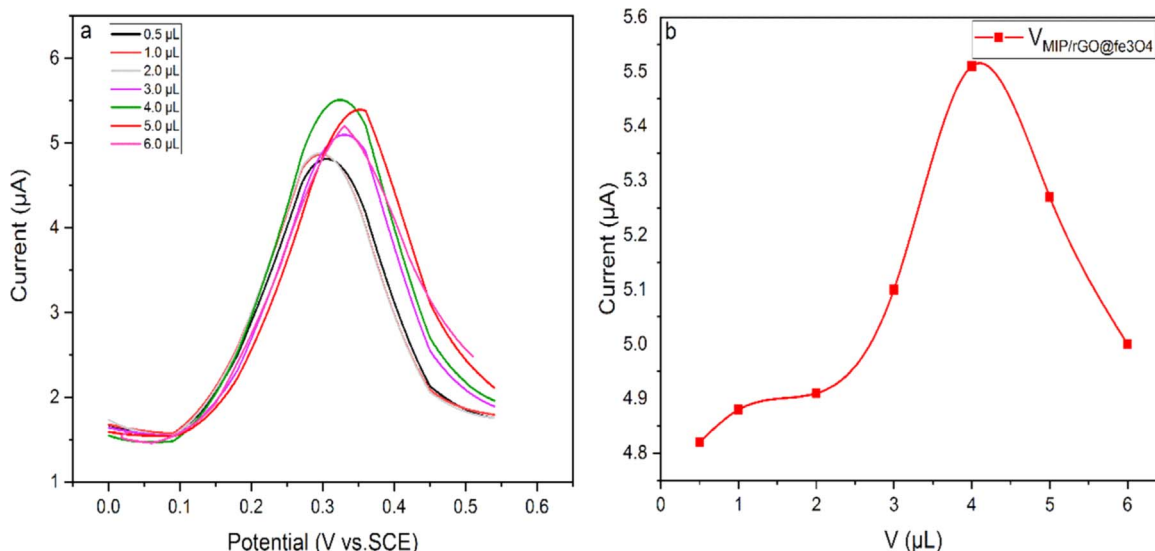
Figure 4. (a), (b) Dosage effect of MIP/rGO@Fe$_3$O$_4$/GCE (μl) of 50 μM CC in 0.1 M PBS at Sweep rate 100 mV s^{-1}.
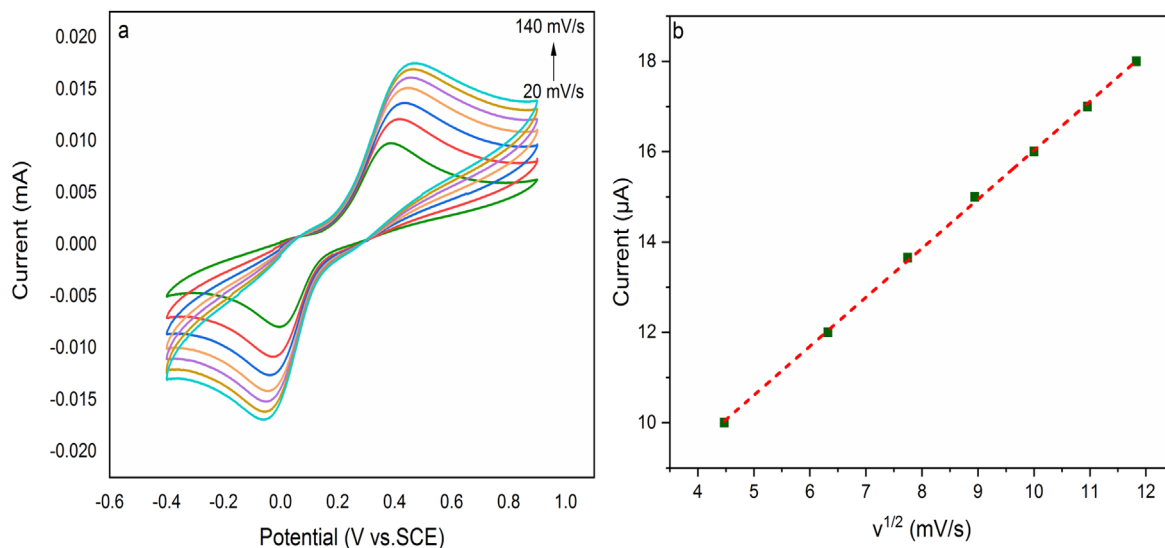
Figure 5. Effect of scan rate range from 20 to 140 mV s^{-1} of 50 μM CC in 0.1 M PBS at MIP/rGO@Fe$_3$O$_4$/GCE.

Figure 6. AP results for MIP/rGO@Fe$_3$O$_4$/GCE in 0.1 M PBS solution in presence of CAc (50 μM), GL (50 μM), HQ (50 μM), DA (50 μM) and CA (50 μM) as molecules of interference.

[Fe(CN)$_6$]$^{3-/4-}$. In Fig. 3, it is noticeable that the NIP/GCE experienced a decrease in current compared with the bare GCE because, in the NIP, the template (CC) already occupied the cavities in polymer contrary to the MIP where the current intensity has been increased drastically due to the extraction of CC from the prepared MIP indicating the high sensitivity and selectivity of the MIP/GCE.

To improve the sensitivity of the MIP/GCE sensing system, MIP nanomaterials were combined with an organic-inorganic nanohybrid namely rGO@Fe$_3$O$_4$ in a 1/1 ratio (3 mg ml^{-1}). As can be seen in the Fig. 3, MIP/rGO@Fe$_3$O$_4$/GCE network sensing system showed good electrochemical performance compared to bare GCE, MIP/GCE and rGO@Fe$_3$O$_4$/GCE. This good electrochemical performance of MIP/rGO@Fe$_3$O$_4$/GCE may due to the outstanding electrocatalytic activity of the synthesized rGO@Fe$_3$O$_4$,and the synergic effect between rGO@Fe$_3$O$_4$ and MIP.

Amount of MIP/rGO@Fe$_3$O$_4$/GCE effect.—To optimize the amount of the MIP/rGO@Fe$_3$O$_4$, we drop-casted different volumes ranging from 0.5 to 6 μl of MIP/rGO@Fe$_3$O$_4$ on the GCE surface. The Fig. 4 shows that the current intensity has been increased dramatically from 0.5 μl to 4.0 μl of MIP/rGO@Fe$_3$O$_4$ where an optimum was reached. Further, above 4 μl of MIP/rGO@Fe$_3$O$_4$, we observed current intensity decrease due to the side effect of huge-thickness of the drop-cased matrix on the GCE surface. Hence, in the next section of this study; a volume of 4 μl of MIP/rGO@Fe$_3$O$_4$ has been drop-casted on the GCE as an optimum volume.

Scan rate effect on MIP/rGO@Fe$_3$O$_4$/GCE.—To investigate the scan rate effect of the MIP/rGO@Fe$_3$O$_4$/GCE, various values from 20 to 140 mV s^{-1} have been applied as shown in Fig. 5a. The results obtained depict that the current peaks and the sweep rate are in linear correlation following the equation: Current (μA) = $5.15 \times V^{1/2}\left(\frac{mV}{s}\right)$ $+1.084$ with correlation coefficient (R^2) of 0.99946. Those results indicate that the electrochemical oxidation of CC is adsorption-controlled electrochemical processes on the MIP/rGO@Fe$_3$O$_4$/GCE with no side reaction.[41]

Table I. Comparison of catechol sensors based on rGO.

Sensor Matrix	LOD (nM)	LR (μM)	Sensitivity (μA.mM cm^{-2})	References
ZnO/RGO	47 nM	15–225	162.04	42
N, RGO/ZnO/Au	10	2–600	/	43
MnO$_x$/rGO	28	0.5–200	/	44
N, P-rGO	99.7	1–100	/	45
TiO$_2$-ZnO-rGO	45	0.1–500	/	46
MIP/rGO@Fe$_3$O$_4$	4.18	1–50	0.0918	This work
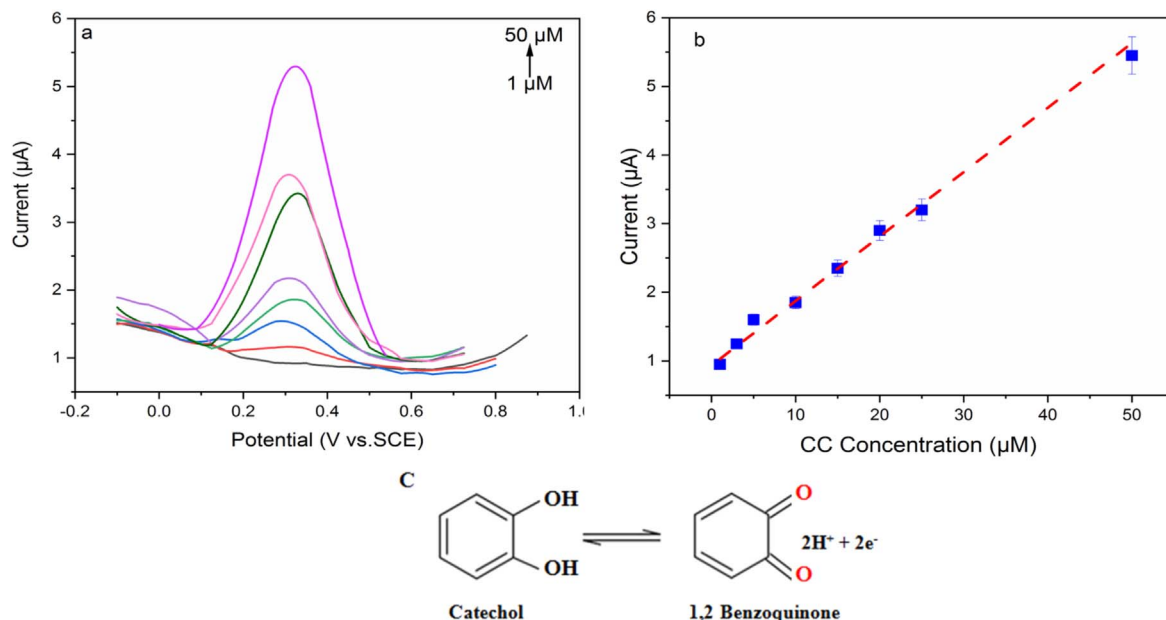
Figure 7. (a) DPV responses for the standard addition of CC in 0.1 M PBS (pH 7.0) at MIP/rGO@Fe$_3$O$_4$/GCE. (b) Linear plot of peak current response against concentration of CC. (c) Reaction mechanism of CC on the MIP/rGO@Fe$_3$O$_4$/GCE.

Selectivity studies.—50 μM of dopamine (DA), hydroquinone (HQ), glucose (Gl), citric acid (CA) and cafeic acid (CAc) have been used as interferences to study the sensor's selectivity by Amperometery (AP) due to its sensitivity, short time response and operation accuracy. The results obtained have been recorded and presented in Fig. 6. Compared to other interferences; The MIP/rGO@Fe$_3$O$_4$/GCE exhibited higher affinity towards CC. These results indicate that the sensor prepared in the present work could be very useful for the detection of CC with the presence of other similar molecules with good sensitivity and selectivity.

Sensitivity of MIP/rGO@Fe$_3$O$_4$.—The electrochemical detection of CC has been performed based on MIP/rGO@Fe$_3$O$_4$/GCE using DPV technique has been used because of its high sensitivity and efficiency. The DPV responses of MIP/rGO@Fe$_3$O$_4$/GCE towards CC detection are recorded. In this section, CC determination is carried out at different solution concentrations ranging from 1 to 50 μM CC and the findings are highlighted in Fig. 7a. As highlighted in Fig. 7a, an increase in the current intensity of the produced sensor with the standard addition of CC in the solution has been recorded. This increase may be attributed to the successful imprinting of CC to the MIP synthesized leading to this sensitive and selective interaction. The linearity between current response changes and CC concentrations is presented in Fig. 7b, this correlation is expressed in the equation: I(μA) = 0.092 × C(μM)+0.93. The MIP/rGO@Fe$_3$O$_4$/GCE showed outstanding electrocatalysis toward CC ranging from 1 to 50 μM(R^2 = 0.996). The LOD of the MIP/rGO@Fe$_3$O$_4$/GCE has been estimated be around 4.18 nM (S/N = 3) while the limit of quantification was in the range of

12.69 nM. Furthermore, we have made a comparative investigation of the analytical performance of MIP/rGO@Fe$_3$O$_4$/GCE with other modified electrodes based on LOD and linear range as highlighted in Table I. Based on the findings, we can clearly conclude that MIP/rGO@Fe$_3$O$_4$ is an outstanding material for detection of hazardous pollutant CC. The electrochemical reaction mechanism of the CC molecule is proposed in Fig. 7C; thus, we can suggest that this molecule was converted to quinone by the release of two protons that were involved in the redox reaction.[2]

Stability, reproducibility and repeatability of the prepared sensor.—The stability of the MIP/rGO@Fe$_3$O$_4$/GCE was investigated in 50 μM of CC using CV as shown in Fig. 8a. A decrease of 4.4% in the response current of the sensor has been occurred suggesting that the MIP/rGO@Fe$_3$O$_4$ has high stability to CC detection even after 30 cycles. The reproducibility (Fig. 8b) and repeatability (Fig. 8c) of MIP/rGO@Fe$_3$O$_4$/GCE was examined by the determination of 50 μM CC. The RSD was determined to be 3.45% and 3.65%, showing that the sensor possessed good reproducibility and repeatability.

Applicability of the electrochemical sensor.—To investigate the applicability of the MIP/rGO@Fe$_3$O$_4$/GCE, local tap water and commercial milk have been used as real samples without any treatment. As highlighted in Table II, the recoveries obtained were in the range of 93.33%–96% and 92%–100% for a sample of tap water and another one of commercial milk respectively. These findings confirm the importance of the developed sensor to detect the presence of CC in real beverage samples.

Table II. Recoveries of CC in a local tap water and commercial milkat MIP/rGO@Fe$_3$O$_4$/GCE.

Real-Sample	Analyte	Added (μM)	Detected (μM)	Recoveries (%)
		00	00	—
Tap Water	CC	15	14	93.33
		50	48	96
		00	00	—
Commercial milk	CC	15	15	100
		50	46	92
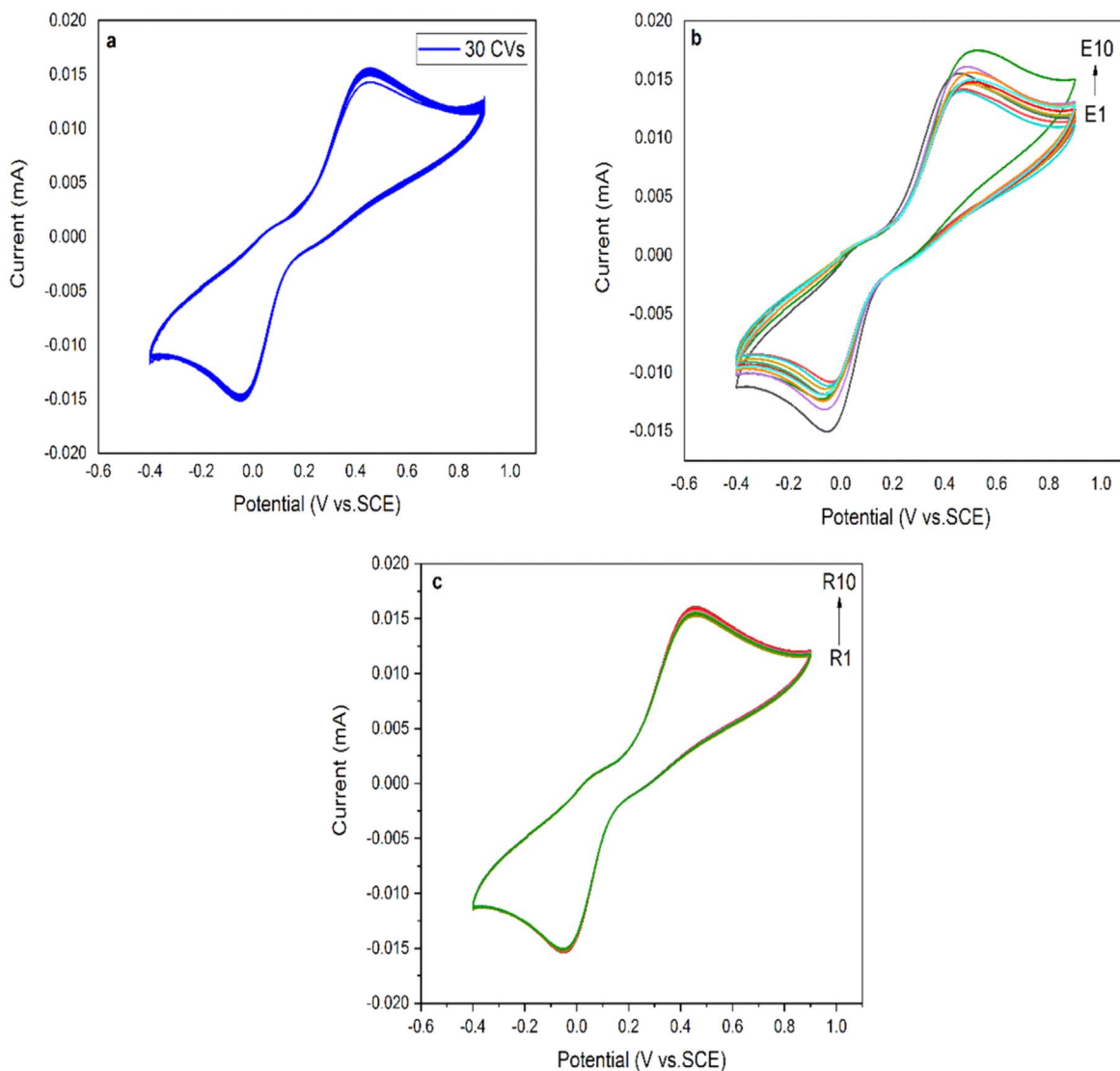
Figure 8. (a) Stability of 30 CVs, (b) reproducibility and (c) repeatability of the MIP/rGO@Fe$_3$O$_4$/GCE.

Table III. Settings and the key parameters of the ANN model.

CC ANN	
Inputs	Concentrations
Output	Electrochemical response
Layers	3
Hidden Layer	2
Hidden Neurons	5
Transfer functions	Logsig/Logsig/purelin
Train function	Traingdm
Learning rate	0.1 (10%)
epochs	8000
Error	10^{-30}
Minimum error achieved	2.6607×10^{-12}
Best performance	778 epochs

ANN preparation.—Herein, the ANN has been developed using the neural network toolbox in MATLAB 6.1 for more accurate identification of CC. The ANN contains three layers. The first layer which is the input layer represents analyte responses where the output layer represents CC concentrations. The settings and the key parameters of the ANN model are shown in Table III. The model was trained until a minor error was achieved. The model is able to estimate CC concentration ranging from LOD (4.18 nM) to 50 M with high accuracy. For the training of the ANN with a maximum weight of neurons in the hidden layers, the Levenberg-Marquardt approach is applied while eight concentrations of CC (1–50 μM) have been used as inputs of the model. The best validation performance of the ANN is presented in Fig. 9.

Figure 10 depicts the results obtained from the training of the ANN. The R-value of the correlation factor represents the link between the outputs and the CC concentration objectives. The training data demonstrate the suitability of the approach to the CC sensor. The R-value for the validation and test data is also quite high. The scatter graphs show that the built ANN in this study achieves excellent fitting. Specific CC concentrations chosen at random between the 4.18 nM and 50 μM have been used to test the performance of the ANN. The results of each test are summarized in Table IV. As demonstrated in Fig. 11, the model can predict CC concentrations with a minimal error despite the limited input data available for training the ANN. These results are encouraging since basic electrochemical measurements of anodic current combined with ANN-based data processing allow for the detection of pollutants as well as a relatively accurate estimation of their amounts.
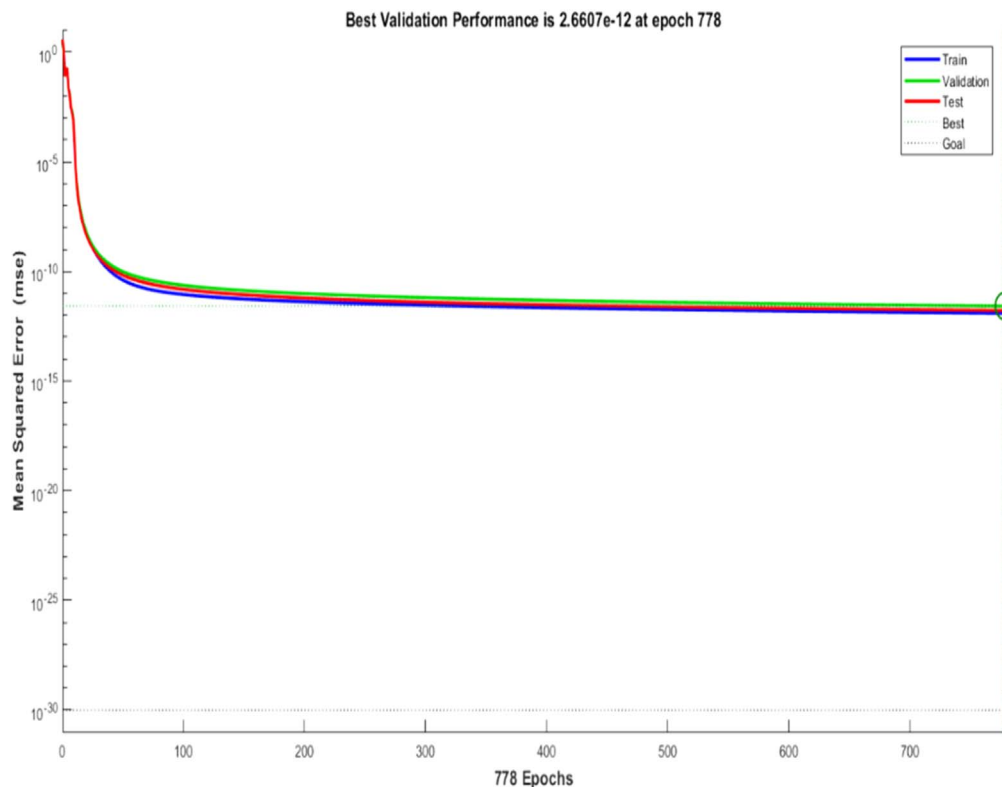
Figure 9. Best validation performance of the ANN.

Table IV. Comparison between the real and estimated CC concentrations using the developed ANN.

CC concentration (μM)	CC oxidation current (μA)	Predicted CC oxidation current (μA)
0.00418 lOD	Not Applicable (N/A) at the laboratory	0.9304
0.01	N/A	0.9309
0.05	N/A	0.9346
0.1	N/A	0.9392
0.3	N/A	0.9576
0.5	N/A	0.9760
0.75	N/A	0.9990
1	0.91	1.0220
2	1.16	1.1140
5	1.56	1.3900
10	1.88	1.8500
15	2.25	2.3100
20	2.9	2.7700
25	3.22	3.2300
50	5.54	5.5300

Conclusions

The present study reports novel green extraction and reduction procedures of MIP and GO, respectively. The novel MIP/rGO@Fe$_3$O$_4$ nanocomposite exhibited outstanding electrochemical performance toward CC detection. The nanocomposite could specifically improve the GCE sensitivity, which resulted in an increase of the peak current intensity of ferricyanide using the modified electrode. The MIP/rGO@Fe$_3$O$_4$/GCE could detect CC from 1 and 50 μM with a detection limit of 4.18 nM. The prepared sensor is simple to be prepared, stable and has a great selectivity toward CC due to the imprinted cavities in the synthesis MIP. The MIP/rGO@Fe$_3$O$_4$/GCE exhibited several advantages including the ease and the cost-effective preparation procedure and the ability to be used for real beverage samples with very important recoveries.

In addition, the current study described how to apply ANN to solve the sensor's problem with detecting low CC concentrations close to the LOD. Through the use of the ANN in data processing, low-concentration CC may be quickly identified, allowing for real-time monitoring of the pollutant from LOD to 50 μM. Applying ANN may enhance sensor sensitivity and assess data from the actual world.
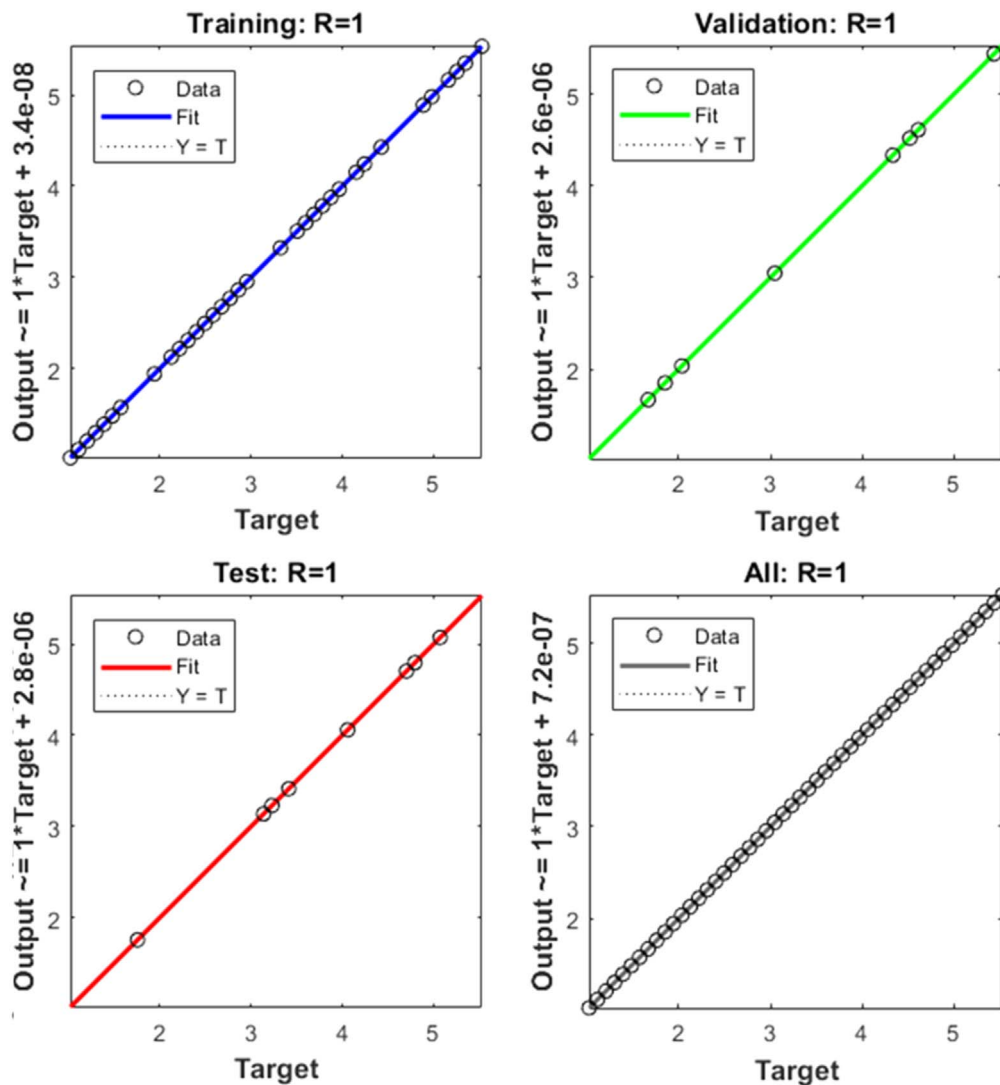
Figure 10. Training performance of the ANN.
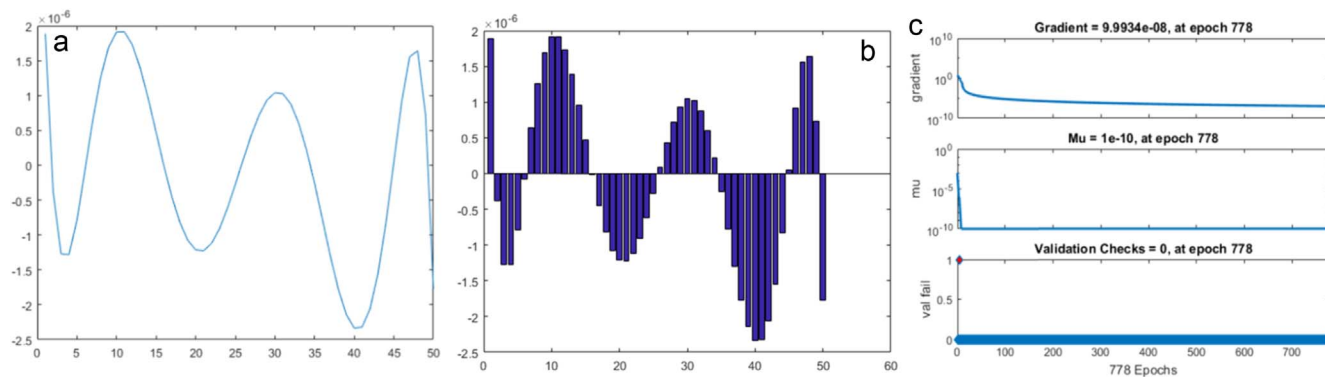
Figure 11. (a), (b) ANN prediction error; (c) Gradient and failure rate of the developed ANN.

ORCID

Hicham Meskher ⓘ https://orcid.org/0000-0002-6097-9439
Fariborz Sharifianjazi ⓘ https://orcid.org/0000-0001-8410-8868

References

1. Z. Lu et al., "Bimetallic MOF synergy molecularly imprinted ratiometric electrochemical sensor based on MXene decorated with polythionine for ultra-sensitive sensing of catechol." *Anal. Chim. Acta*, **1251**, 340983 (2023).
2. A. de, S. M. de Freitas, C. C. Maciel, A. P. Lemes, and M. Ferreira, "Thermoplastic starch and graphite biocomposite electrode for electrochemical catechol sensor." *ECS Adv.*, **1**, 036504 (2022).
3. L. Liao et al., "Electrochemical sensor based on Ni/N-doped graphene oxide for the determination of hydroquinone and catechol." *Ionics*, **29**, 1605 (2023).

4. J. Zuo et al., "Flexible electrochemical sensor constructed using an active copper center instead of unstable molybdenum carbide for simultaneous detection of toxic catechol and hydroquinone." *Microchem. J.*, **187**, 108443 (2023).

5. M. K. Abugazleh, H. M. Ali, J. A. Chester, and J. L. Bouldin, "Aquatic toxicity of hydroquinone and catechol following metal oxide treatment to ceriodaphnia dubia and pimephales promelas." *In Review*, **1**, 1 (2022).

6. V. Parrales-Macias et al., "Effects of a new natural catechol- *O* -methyl transferase inhibitor on two in vivo models of parkinson's disease." *ACS Chem. Neurosci.*, **13**, 3303 (2022).

7. H. Li et al., "Detection of catecholamine metabolites in urine based on ultra-high-performance liquid chromatography–tandem mass spectrometry." *Biomed. Chromatogr.*, **36**, 3 (2022).

8. M. Abualhasan, F. Shraim, H. Alawni, S. Hamdan, and H. Khaseeb, "HPLC analytical method development and validation of gabapentin through chemical derivatization with catechol as a chromophore." *Int. J. Anal. Chem.*, **2022**, 1 (2022).

9. L. Della Vedova et al., "Liquid chromatography–high-resolution mass spectrometry (LC-HRMS) profiling of commercial enocianina and evaluation of their antioxidant and anti-inflammatory activity." *Antioxidants*, **11**, 1187 (2022).

10. R. Pillai, S. Preetha, B. Narasimhamurthy, and I. C. Lekshmi, "Biosensing of catechol via amperometry using laccase immobilized nickel oxide/graphite modified screen-printed electrodes." *Mater. Today Proc.*, **62**, 5434 (2022).

11. X. Wu et al., "Lignin-first monomers to catechol: rational cleavage of C−O and C−C bonds over zeolites." *ChemSusChem*, **15**, 7 (2022).

12. J. Veenhoven, H. van Keulen, S. Saverwyns, F. Lynen, and M. van Bommel, "Optimising the analysis of Anacardiaceae (Asian lacquer) polymers using pyrolysis-gas chromatography-mass spectrometry." *J. Anal. Appl. Pyrolysis*, **170**, 105845 (2023).

13. R. Hossain, K. Hassan, and V. Sahajwalla, "Utilising problematic waste to detect toxic gas release in the environment: fabricating a NiO doped CuO nanoflake based ammonia sensor from e-waste." *Nanoscale Adv.*, **4**, 4066 (2022).

14. A. S. Dahiya et al., "Review—energy autonomous wearable sensors for smart healthcare: a review." *J. Electrochem. Soc.*, **167**, 037516 (2020).

15. H. Meskher et al., "A review on CNTs-based electrochemical sensors and biosensors: unique properties and potential applications." *Crit. Rev. Anal. Chem.*, 1 (2023).

16. R. Gui, H. Guo, and H. Jin, "Preparation and applications of electrochemical chemosensors based on carbon-nanomaterial-modified molecularly imprinted polymers." *Nanoscale Adv.*, **1**, 3325 (2019).

17. I. Haq et al., "Determination of sitagliptin in human plasma using a smart electrochemical sensor based on electroactive molecularly imprinted nanoparticles." *Nanoscale Adv.*, **3**, 4276 (2021).

18. P. Manickam, S. K. Pasha, S. A. Snipes, and S. Bhansali, "A reusable electrochemical biosensor for monitoring of small molecules (cortisol) using molecularly imprinted polymers." *J. Electrochem. Soc.*, **164**, B54 (2017).

19. H. Meskher et al., "Recent trends in carbon nanotube (CNT)-based biosensors for the fast and sensitive detection of human viruses: a critical review." *Nanoscale Adv.*, **5**, 992 (2023).

20. A. H. M. Safaryan, A. M. Smith, T. S. Bedwell, E. V. Piletska, F. Canfarotta, and S. A. Piletsky, "'Optimisation of the preservation conditions for molecularly imprinted polymer nanoparticles specific for trypsin." *Nanoscale Adv.*, **1**, 3709 (2019).

21. H. Kaur and M. Shorie, "Nanomaterial based aptasensors for clinical and environmental diagnostic applications." *Nanoscale Adv.*, **1**, 2123 (2019).

22. Y. Hua, D. Kukkar, R. J. C. Brown, and K.-H. Kim, "Recent advances in the synthesis of and sensing applications for metal-organic framework-molecularly imprinted polymer (MOF-MIP) composites." *Crit. Rev. Environ. Sci. Technol.*, **53**, 258 (2023).

23. H. Wu, G. Lin, C. Liu, S. Chu, C. Mo, and X. Liu, "Progress and challenges in molecularly imprinted polymers for adsorption of heavy metal ions from wastewater." *Trends Environ. Anal. Chem.*, **36**, e00178 (2022).

24. S. Yang, Y. Teng, Q. Cao, C. Bai, Z. Fang, and W. Xu, "Electrochemical sensor based on molecularly imprinted polymer-aptamer hybrid receptor for voltammetric detection of thrombin." *J. Electrochem. Soc.*, **166**, B23 (2019).

25. H. Kamyab et al., "A review on carbon-based molecularly-imprinted polymers (CBMIP) for detection of hazardous pollutants in aqueous solutions." *Chemosphere*, **308**, 136471 (2022).

26. Z. Mazouz et al., "Computational approach and electrochemical measurements for protein detection with MIP-based sensor." *Biosens. Bioelectron.*, **151**, 111978 (2020).

27. X. Guo, J. Li, M. Arabi, X. Wang, Y. Wang, and L. Chen, "Molecular-imprinting-based surface-enhanced raman scattering sensors." *ACS Sens.*, **5**, 601 (2020).

28. A. Raziq, A. Kidakova, R. Boroznjak, J. Reut, A. Öpik, and V. Syritski, "Development of a portable MIP-based electrochemical sensor for detection of SARS-CoV-2 antigen." *Biosens. Bioelectron.*, **178**, 113029 (2021).

29. I. Khelfaoui, Y. Xie, M. Hafeez, D. Ahmed, H. E. Degha, and H. Meskher, "Effects of health shocks, insurance, and education on income: fresh analysis using CHNS panel data." *Int. J. Environ. Res. Public. Health*, **19**, 8298 (2022).

30. I. Khelfaoui, Y. Xie, M. Hafeez, D. Ahmed, H. E. Degha, and H. Meskher, "Information communication technology and infant mortality in low-income countries: empirical study using panel data models." *Int. J. Environ. Res. Public. Health*, **19**, 7338 (2022).

31. G. Wang, Q.-S. Jia, M. Zhou, J. Bi, J. Qiao, and A. Abusorrah, "Artificial neural networks for water quality soft-sensing in wastewater treatment: a review." *Artif. Intell. Rev.*, **55**, 565 (2022).

32. N. Noori, L. Kalin, and S. Isik, "Water quality prediction using SWAT-ANN coupled approach." *J. Hydrol.*, **590**, 125220 (2020).

33. N.-G. Lim, J.-Y. Kim, and S. Lee, "Estimation of the hot swap circulation current of a multiple parallel lithium battery system with an artificial neural network model." *Electronics*, **10**, 1448 (2021).

34. Y. Yang, Y. Liu, and X. Zhao, "Preparation and characterization of an electromagnetic composite polypyrrole/polyethylene short filament geotextile." *Text. Res. J.*, **92**, 1333 (2022).

35. A. N. Al-hakimi, F. Alminderej, I. A. Alhagri, S. M. Al-Hazmy, M. O. Farea, and E. M. Abdallah, "Inorganic nanofillers TiO2 nanoparticles reinforced host polymer polypyrrole for microelectronic devices and high-density energy storage systems." *J. Mater. Sci., Mater. Electron.*, **34**, 238 (2023).

36. X. Liang, Y. Liu, Z. Wen, L. Huang, X. Wang, and H. Zhang, "A nano-structured and highly ordered Ppyr-sulfur cathode for lithium–sulfur batteries." *J. Power Sources*, **196**, 6951 (2011).

37. R. Sharma, G. B. V. S. Lakshmi, A. Kumar, and P. Solanki, "Polypyrrole based molecularly imprinted polymer platform for klebsiella pneumonia detection." *ECS Sens. Plus*, **1**, 010603 (2022).

38. L. A. Mohammed et al., "Design and characterization of novel ternary nanocomposite (rGO-MnO2-PoPDA) product and screening its dielectric properties." *Int. J. Interact. Des. Manuf. IJIDeM* (2022).

39. A. Singh, A. Sharma, A. Ahmed, and S. Arya, "Highly selective and efficient electrochemical sensing of ascorbic acid via CuO/rGO nanocomposites deposited on conductive fabric." *Appl. Phys. A*, **128**, 262 (2022).

40. A. Alangari et al., "Iron oxide nanoparticles: preparation, characterization, and assessment of antimicrobial and anticancer activity." *Adsorpt. Sci. Technol.*, **2022**, 1 (2022).

41. Y. Zhu, S. Huai, J. Jiao, Q. Xu, H. Wu, and H. Zhang, "Fullerene and platinum composite-based electrochemical sensor for the selective determination of CC and hydroquinone." *J. Electroanal. Chem.*, **878**, 114726 (2020).

42. R. Ponnusamy et al., "Experimental and density functional theory investigations of catechol sensing properties of ZnO/RGO nanocomposites." *Appl. Surf. Sci.*, **495**, 143588 (2019).

43. J. He, S. Xing, R. Qiu, Z. Song, and S. Zhang, "L -Cysteine/glycine composite film modified glassy carbon electrode as an enhanced sensing platform for catechol determination." *Anal. Methods*, **6**, 1210 (2014).

44. G. Liu et al., "Electrochemical sensor based on laser-induced preparation of MnOx/rGO composites for simultaneous recognition of hydroquinone and catechol." *Microchem. J.*, **185**, 108234 (2023).

45. Y. Liu et al., "A sensitive electrochemical sensor based on dual Co-doped N, P-rGO for simultaneous determination of hydroquinone and catechol." *J. Electrochem. Soc.*, **168**, 017514 (2021).

46. X.-Y. Lu et al., "Facile synthesis of TiO2-ZnO-rGO nanocomposites for highly sensitive simultaneous determination of hydroquinone and catechol." *Microchem. J.*, **166**, 106246 (2021).